Journal of Geochemical Exploration 165 (2016) 111–124

Contents lists available at ScienceDirect

Journal of Geochemical Exploration

journal homepage: www.elsevier.com/locate/gexplo

Recognition of significant multi-element geochemical signatures of porphyry Cu deposits in Noghdouz area, NW Iran

Mohammad Parsa [a], Abbas Maghsoudi [a,*], Mahyar Yousefi [b], Martiya Sadeghi [c]

[a] Faculty of Mining and Metallurgical Engineering, Amirkabir University of Technology, Tehran, Iran
[b] Faculty of Engineering, Malayer University, Malayer, Iran
[c] Mineral Resource Department, Geological Survey of Sweden, Uppsala, Sweden

ARTICLE INFO

Article history:
Received 15 August 2015
Revised 8 March 2016
Accepted 9 March 2016
Available online 12 March 2016

Keywords:
Significant geochemical signatures
Stream sediment geochemical data
Sample catchment basin models
Contour maps
Prediction-area (P-A) plot
Success rate curve

ABSTRACT

Diversity and complexity of geological processes in different areas result in different element associations for prospecting a certain mineral deposit-type sought. In this regard, because element associations are affected by the diversity of geological characteristics of different areas, it is important to analyze and recognize significant geochemical signatures that represent the deposit-type sought. This paper aims to recognize significant multi-element geochemical signatures of porphyry-Cu deposits in the Noghdouz area, Iran, using stream sediment data. For this, we used factor analysis and two modeling methods of geochemical anomalies, sample catchment basin and contour map. Then, to recognize significant geochemical signatures of the deposit-type sought and evaluate the anomaly mapping methods, we adapted prediction-area (P-A) plot, normalized density, and success rate curve. By using these processes, we recognized the best geochemical signature of the deposit-type sought in the study area. The proposed methods in this paper can efficiently be used in other areas to recognize significant geochemical signatures of different types of mineral deposits.

1. Introduction

Maps of geochemical signatures are efficient evidence layers for integration with other exploration evidence layers in mineral prospectivity mapping (MPM) of certain types of deposits (e.g., Agterberg, 1992; Agterberg and Bonham-Carter, 2005; Carranza, 2008, 2011; Lusty et al., 2012; Wang et al., 2012; Liu et al., 2014; Carranza, 2015; Carranza and Laborte, 2015a, 2015b; Yousefi and Carranza, 2016). In preliminary exploration stages, stream sediment geochemical data are generally used to delineate anomalous areas (e.g., Carranza and Hale, 1997; Cheng, 2007; Zuo et al., 2009; Bai et al., 2010; Carranza, 2011; Zuo, 2011b; El-Makky and Sediek, 2012; Zheng et al., 2014; Wang et al., 2014; Wang and Zuo, 2015). For recognizing geochemical signatures related to a certain deposit-type sought, factor analysis (as a multivariate analysis method) has been used (e.g., Reimann et al., 2002; Kumru and Bakac, 2003; Helvoort et al., 2005; El-Makky, 2011; He et al., 2013; Sadeghi et al., 2015). Factor analysis reveals element associations that genetically present in the mineral deposits of the type sought (e.g., Sadeghi et al., 2013; He et al., 2014).

Recognition of significant mineralization-related multi-element geochemical signatures is a challenge, because factor analysis may reveal more than one multi-element association (i.e., factors) representing the same deposit of the type sought. On the other hand, factor analysis may reveal some factors in the chemical composition of stream sediment data that are not genetically related to the deposit-type sought (Yilmaz, 2003; Spadoni, 2006; Cheng, 2007; Zuo et al., 2009; Xie et al., 2010; Yousefi et al., 2012).

Modeling of geochemical anomalies especially in stream sediment data is another challenging issue because the materials of each stream sample have upstream sources (Spadoni, 2006; Carranza, 2008). In this regard, several methods have been proposed for mapping stream sediment geochemical signatures including point symbol maps, contour mapping or interpolation approaches (Howarth, 1983), sample catchment basins (SCB) (Bonham-Carter and Goodfellow, 1984, 1986; Bonham-Carter, 1994; Carranza and Hale, 1997; Moon, 1999; Spadoni et al., 2004; Carranza, 2008; Carranza, 2010b), stream orders (Carranza, 2004), extended sample catchment basins (Spadoni, 2006) and weighted drainage catchment basins (Yousefi et al., 2013). Various studies have applied contour mapping and SCB for modeling geochemical anomalies using stream sediment data (e.g., Hawkes, 1976; Bonham-Carter et al., 1987, 1988; Carranza, 2004, 2008, 2010a).

This study aims to recognize significant multi-element geochemical signatures and map geochemical anomalies associated with porphyry-Cu deposits to delineate target areas for further exploration in the Noghdouz area, northwestern Iran. For this, we used staged factor analysis proposed by Yousefi et al. (2012, 2014) with robust estimation of covariance matrix (Pison et al., 2003; Filzmoser et al., 2009b). We

* Corresponding author at: Amirkabir University of Technology, Tehran, Iran.
E-mail address: a.maghsoudi@aut.ac.ir (A. Maghsoudi).

http://dx.doi.org/10.1016/j.gexplo.2016.03.009
0375-6742/

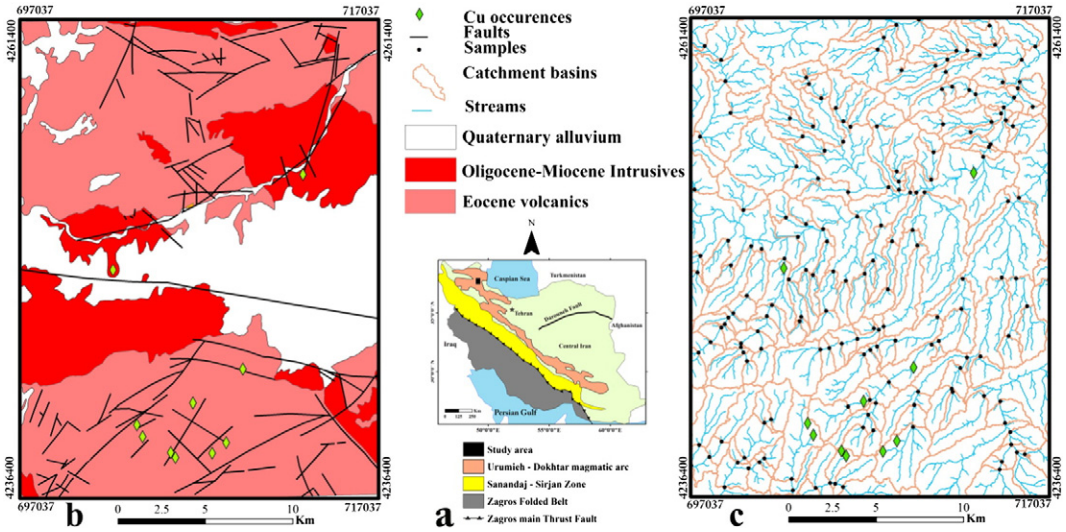

Fig. 1. (a) Location of the study area in Urumieh–Dokhtar magmatic belt, (b) simplified geological map of the study area (after Mahdavi and Amini Fazl, 1988) and (c) the location of samples and their related catchment basins.

applied SCB and contour mapping methods to model anomalies. For selecting a stronger geochemical evidence layer of the deposit-type sought in the study area, we compared the results of integration of both SCB model and contour map with another geological evidence layer in MPM. We used two models because different areas have different characteristics and complexity (Ford and Blenkinsop, 2008; Van Loon, 2002), so at least two different models should be generated and compared in an area to select the better model for MPM (e.g., Harris et al., 2003; Yousefi and Carranza, 2015c). In this paper, for recognition of significant multi-element geochemical signatures we used the location of 10 known mineral occurrences in the study area (e.g., Agterberg and Bonham-Carter, 2005; Porwal et al., 2003, 2004, 2006; Yousefi et al., 2012, 2013, 2014; Carranza and Laborte, 2015c; Gholami et al., 2012). These deposits were utilized only as testing points for assessing the ability of generated models to predict the presence of mineral deposits. Prediction-area (P-A) plot (Yousefi and Carranza, 2015a, 2015b, 2015c), normalized density (Mihalasky and Bonham-Carter, 2001; Yousefi and Carranza, 2015b) and success rate curve (Chung and Fabri, 2003; Agterberg and Bonham-Carter, 2005) as modified by Parsa et al. (2016) were utilized for evaluating multi-element geochemical signatures derived by robust staged factor analysis.

2. The study area and porphyry copper mineralization

The study area is situated in the northern part of Urumieh–Dokhtar magmatic arc (UDMA) (Fig. 1a). The UDMA is an Andean type magmatic arc (Berberian et al., 1982), which has been formed by the subduction of Arabian plate beneath Central Iran during the Alpine orogeny in the Late Cretaceous (Berberian and King, 1981; Mohajjel and Fergusson, 2000; Babaie et al., 2001). Porphyry-Cu deposits show a strong tendency to form in island and continental-arc settings (e.g., UDMA) (Billa et al., 2004; Cooke et al., 2005; Mitchell, 1973; Sillitoe, 1972, 2010). The exploration results and known mineral occurrences in the UDMA indicate that this belt has great potential for prospecting porphyry-Cu deposits in Iran (e.g., Richards et al., 2012; Ayati et al., 2013; Zarasvandi et al., 2015).

The study area with a surface of ~600 km^2 is covered by 1:50,000 scale quadrangle map of Noghdouz. Quaternary alluvial deposits,

Table 1
Rotated component matrix of the first and second stages of robust factor analysis. Loadings in bold represent the selected elements based on the absolute threshold value of 0.5.

First stage					Second stage			
Element	F1	F2	F3	F4	Element	F1	F2	F3
Au	**−0.559**	−0.229	−0.229	−0.111	Au	**0.569**	−0.625	−0.317
Cr	0.281	−0.124	0.252	**0.519**	Ag	**0.54**	−0.619	−0.342
Mn	−0.136	**0.873**	0.112	0.274	As	−0.165	**0.869**	0.145
Ba	0.267	**0.601**	0.234	0.113	Cu	**0.719**	−0.561	−0.286
Ag	**−0.557**	−0.292	−0.266	−0.121	Mo	**0.765**	−0.322	0.121
As	0.121	0.211	**0.8**	−0.194	Pb	−0.729	−0.221	**0.629**
Co	−0.127	0.211	−0.112	**0.837**	Sb	−0.125	**0.651**	0.114
Cu	**−0.65**	−0.216	−0.254	−0.1	Zn	−0.671	−0.182	**0.868**
Mo	**−0.627**	−0.168	−0.243	−0.133	Var.	32.9	30.1	19.2
Ni	0.112	−0.114	−0.196	**0.89**	Cum. Var.	32.9	63	82.1
Pb	**0.777**	0.247	0.126	−0.269				
Sb	0.302	−0.213	**0.731**	−0.219				
Zn	**0.514**	0.194	0.11	0.102				
Sn	0.248	**0.515**	0.212	−0.133				
W	0.295	**0.717**	0.278	−0.231				
Var.	32.6	20.1	15.3	14.4				
Cum. Var.	32.6	52.7	68	82.4				

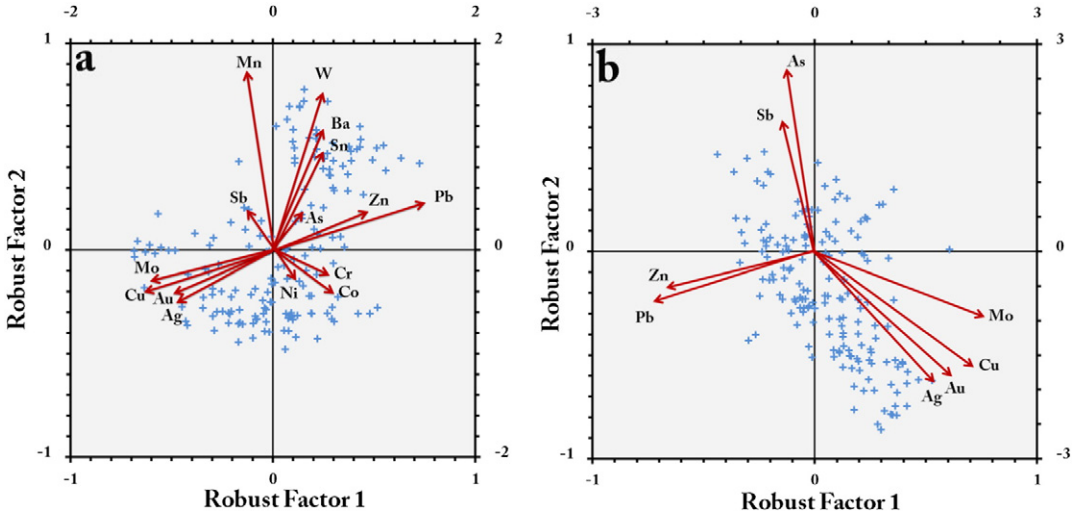

Fig. 2. Biplots of the first and second factors for the first (a) and second (b) stages of robust factor analysis.

Eocene volcanic rocks (i.e., andesites, trachyandesites and porphyritic andesites) and Oligocene intrusive rocks (i.e., granodiorites and quartz-monzonites) are main lithological units of the study area (Mahdavi and Amini Fazl, 1988) (Fig. 1b). The intrusion of Oligocene intrusive rocks into the Eocene volcanic rocks has made a fitting spot for porphyry-Cu mineralization in the study area (Ghorbani, 2013).

3. Methods and results

3.1. Sampling and analysis

The results of chemical analyses of 174 stream sediment samples for 15 elements (Cu, Mo, Pb, Zn, Au, Mn, Ag, Co, Ni, As, Sb, Sn, W, Ba, Cr),

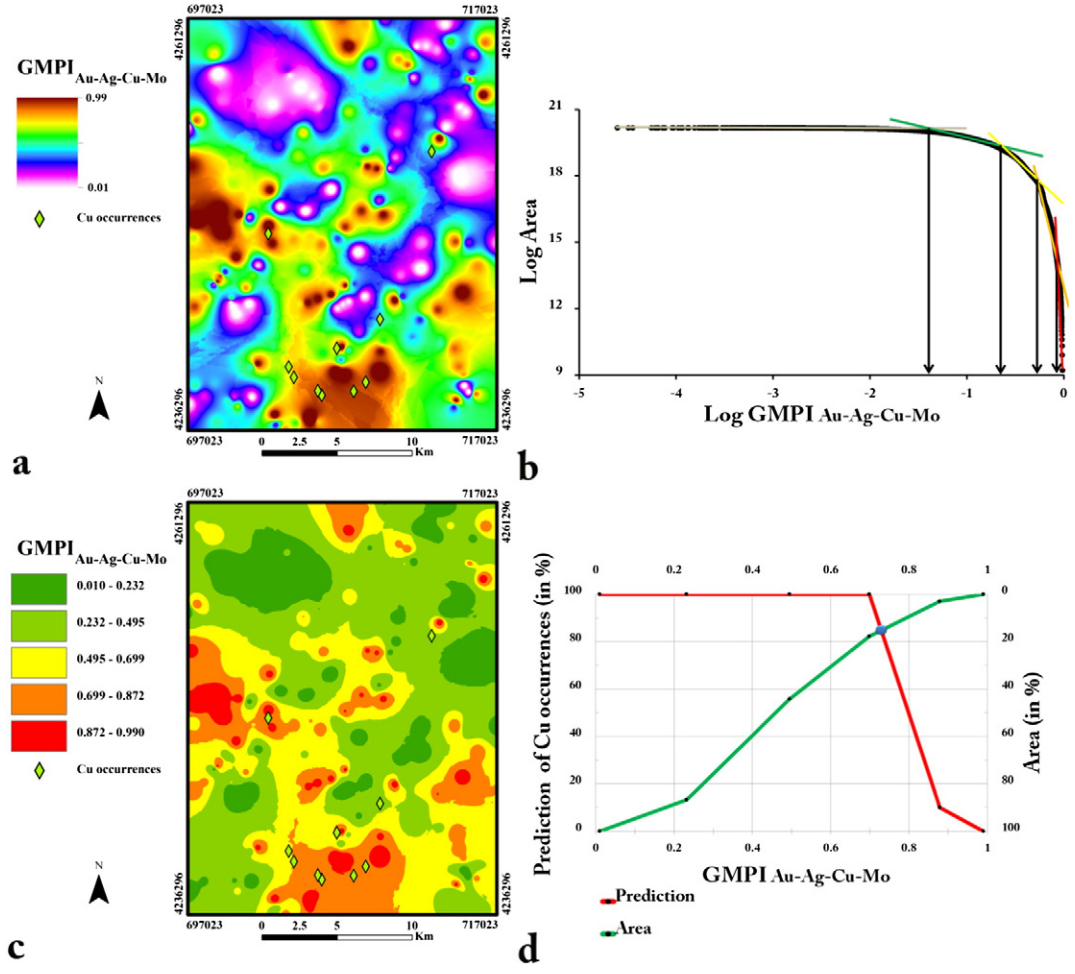

Fig. 3. Interpolated (contour) map of the $GMPI_{Au-Ag-Cu-Mo}$ values (a), C-A fractal model (b), classified map (c), and P-A plot (d).

collected by the Geological Survey of Iran (GSI), were used in this study (Fig. 1c). The samples were sieved by 176 μm screen and the fractions <176 μm were selected for chemical analysis. The sieved fractions were digested in HNO_3 + HCL and then analyzed for multi-elements by inductively coupled plasma optical emission spectrometry (ICP-OES). For measuring Au, fire assay method was employed and the resulted aliquot was analyzed by atomic absorption spectrometer (AAS). The detection limits were: 0.2 ppm for Cu, 0.1 ppm for Mo, 0.2 ppm for Pb, 0.2 ppm for Zn, 1 ppb for Au, 2 ppm for Mn, 0.01 ppm for Ag, 0.2 ppm for Co, 2 ppm for Ni, 0.5 ppm for As, 0.1 ppm for Sb, 0.2 ppm for Sn, 0.1 ppm for W, 0.2 ppm for Ba, and 2 ppm for Cr. The method of Thompson and Howarth (1976) was applied for assessing the analytical precision using duplicated samples. The precision was better than 10% for most of the selected elements.

3.2. Deriving multi-element geochemical signatures

Stream sediment geochemical data are compositional (closed) data, meaning that they represent a closed number system in which individual variables are parts of a whole (Aitchison, 1986; Aitchison and Egozcue, 2005; Filzmoser et al., 2009a; Carranza, 2011). Therefore, in order to open the closed data prior to FA, the data should be log-ratio transformed (Aitchison, 1986; Egozcue et al., 2003; Filzmoser et al., 2009a, 2009b, 2009c; Buccianti and Grunsky, 2014; Buccianti, 2015; Buccianti et al., 2015). Furthermore, due to the effects of several geological events (e.g., mineralization) and their complexities, stream sediment data are heterogeneous and spoiled by outliers (Reimann and Filzmoser, 2000). Thus, robust factor analysis (RFA) should be applied to focus on the major data structure rather than outliers and inhomogeneities (Filzmoser et al., 2009b). In this regard, FA could be optimized by robust estimation of covariance matrix (Pison et al., 2003; Filzmoser et al., 2009b).

There are three log-ratio transformation methods for opening closed data, namely additive log-ratio (alr) (Aitchison, 1986), centered log-ratio (clr) (Aitchison, 1986), and isometric log-ratio transformation (ilr) (Egozcue et al., 2003). Because of symmetric results (Aitchison, 1986), and the feasibility of interpretation of resulting values (Filzmoser et al., 2009b), the clr transformation is appropriate for opening compositional data prior to multivariate analyses. However, the clr transformation results in singularity of data and robust statistical procedures (e.g., minimum covariance determinant (MCD)) could not be applied directly to singular data (Egozcue et al., 2003). Therefore, following Filzmoser et al. (2009b), ilr transformation was initially used to obtain a robust estimation of covariance matrix. The resultant covariance matrix was back-transformed to clr space and was used for deriving loadings and factor scores. In this regard, the interpretation of results of RFA refers to the clr space (Filzmoser et al., 2009b) and is possible via compositional biplots (Aitchison and Greenacre, 2002).

In order to obtain representative multi-element geochemical signatures in the results of RFA, we performed staged factor analysis (Yousefi et al., 2012, 2014). For this, by performing a two staged RFA on clr-transformed data, and by following Filzmoser et al. (2009b), we

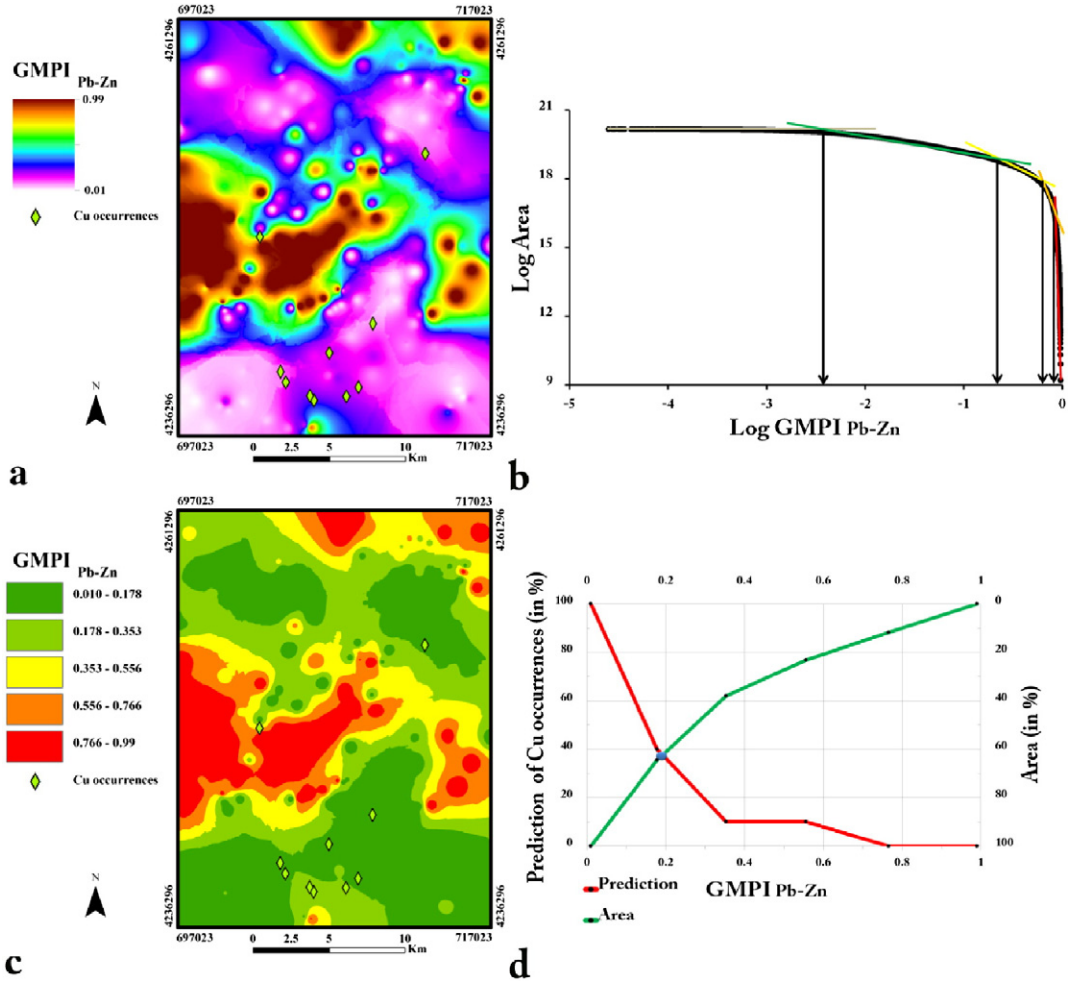

Fig. 4. Interpolated (contour) map of the $GMPI_{Pb-Zn}$ values (a), C-A fractal model (b), classified map (c), and P-A plot (d).

obtained significant multi-element geochemical signatures. The staged factor analysis allows for improved identification of significant anomalous geochemical signatures of the deposit-type sought (Yousefi et al., 2012, 2014). Principle factor analysis (PFA) and varimax rotation of factors (Kaiser, 1958) were used in the two stages of RFA on the clr-transformed data (Reimann et al., 2002). Moreover, the Bartlett method was used for obtaining factor scores (FSs) (e.g., Filzmoser et al., 2009b). We used the R free software for all the statistical analyses in this paper (R Development Core Team, 2008).

In the first stage of RFA, the number of factors was set to be 4 because as Treiblmaier and Filzmoser (2010) mentioned it can be selected based on a significant amount of variance to be explained by the factors. Consequently, we obtained (1) a significant total percentage variability of 82.4% (Table 1) and (2) a proper discrimination of different element associations via these factors. In addition, a threshold loading value should be selected for interpretation of factors. For this, loadings in the range of 0.3 to 0.6 can be used (Borovec, 1996; Chandrajith et al., 2001; Helvoort et al., 2005; Treiblmaier and Filzmoser, 2010; Yousefi et al., 2014). In this regard, we used the absolute value of 0.5 as threshold loading for returning significant factors (e.g., Sun et al., 2009) because 0.5 is a medium value which allows both the slightly and strongly high values to be incorporated in the interpretation of factors. Furthermore, this threshold value allowed us to recognize and discriminate both of the non-mineralization and mineralization related factors. The results of the first stage of the RFA are shown in Table 1. The first factor explains 32.6% of total variability and represents an Au–Ag–Cu–Mo elemental association with negative loadings, while it represents a Pb–Zn elemental association with positive loadings (Table 1). In the second factor, robust positive loadings reflect a Mn–Ba–Sn–W elemental association. In factors 3 and factor 4, robust positive loadings reflect As–Sb, and Cr–Ni–Co associations, respectively. The compositional biplots (e.g., Grunsky, 2010; Levitan et al., 2015) of the first and second factors of the first stage of the RFA (Fig. 2a) reflect several element associations including Au–Ag–Cu–Mo, Cr–Ni–Co, and Pb–Zn. In order to obtain more reliable factor scores indicating porphyry-Cu deposits, as Yousefi et al. (2012, 2014), the data of Cr, Ni and Co, which show a strong association in factor F4, were excluded from the next stage RFA because this association is largely due to lithological variation. Likewise, the data of Mn, Ba, Sn and W, which show strong contributions in factor F2, were excluded from the next stage RFA because these elements are not strong indicators of porphyry-Cu mineralization (Sillitoe, 2010). Thus, the second stage RFA was applied on clr-transformed data of the remaining elements, namely Au, Ag, Cu, Mo, As, Sb, Pb and Zn, all of which are among the most important indicators of porphyry-Cu deposits (Singer et al., 2005; Sotnikov et al., 2007; Qu et al., 2007; Yang et al., 2009; Sillitoe, 2010; Maghsoudi et al., 2014). In the second stage RFA, based on a significant amount of total variance to be explained by factors (Treiblmaier and Filzmoser, 2010), the number of factors was set to be 3 which resulted in a significant total percentage variability of 82.1% (Table 1), and allowed a reasonable discrimination among the elemental associations. In the first, second and third factors of the second stage RFA, the robust positive loadings reflect Au–Ag–Cu–Mo, As–Sb,

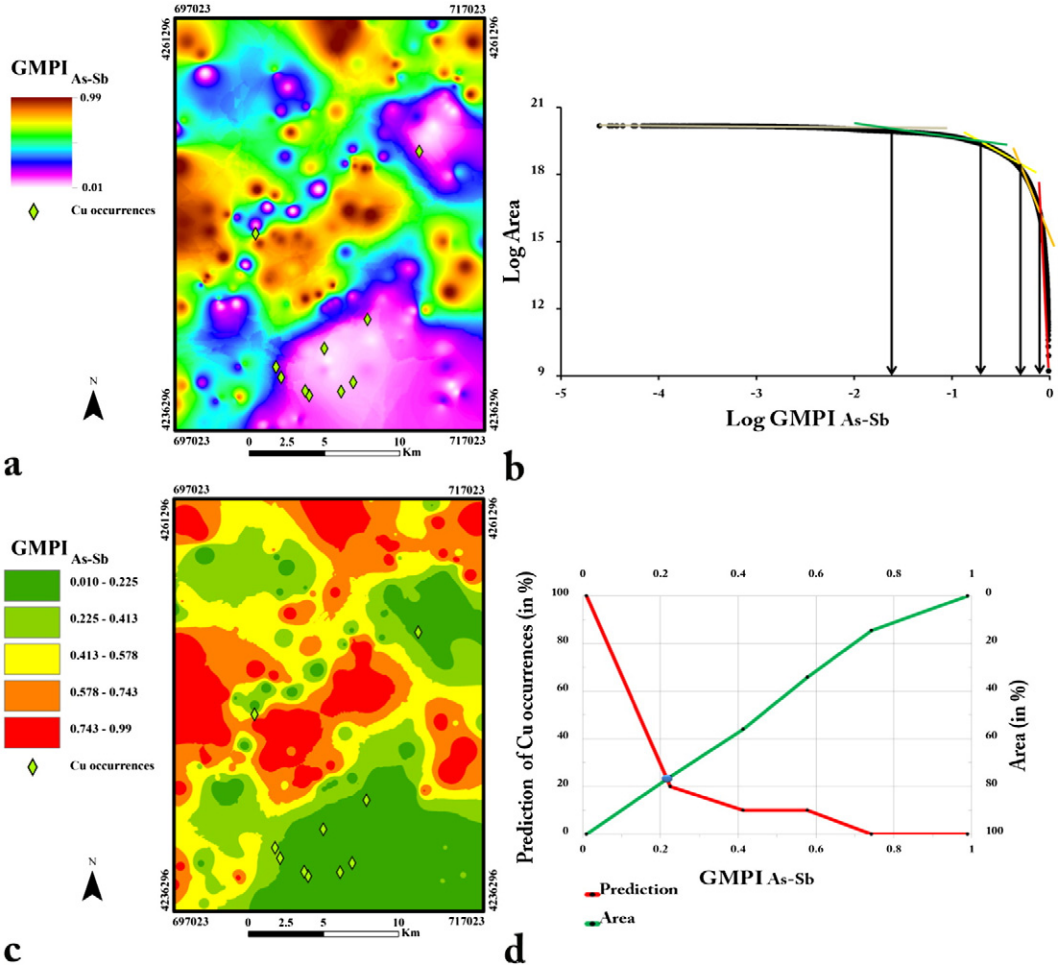

Fig. 5. Interpolated (contour) map of the $GMPI_{As-Sb}$ values (a), C-A fractal model (b), classified map (c), and P-A plot (d).

and Pb–Zn associations, respectively (Table 1). The biplots of the first and second factors of the second stage RFA (Fig. 2b) explicitly illustrate the three elemental associations. Consequently, from the results of the staged RFA, three sets of FSs were obtained: 1) FSs of Au–Ag–Cu–Mo indicator factor, 2) FSs of As–Sb indicator factor, and 3) FSs of Pb–Zn indicator factor.

After obtaining the FSs of the three indicator factors, we transformed them into [0,1] range using a logistic function. Transformation of values of geochemical signatures into [0,1] range using logistic functions compared to original raw values (i.e., FSs) not only allows for better discrimination of geochemical populations, but also improves the prediction rate of MPM (Yousefi et al., 2012, 2014; Yousefi and Carranza, 2015a, 2015b, 2015c). For this, the Eq. [1] of Yousefi and Carranza (2015a) was used for the transformation of each of the three sets FSs values into [0,1] range, here termed geochemical mineralization prospectivity index (GMPI), namely, $GMPI_{Au-Ag-Cu-Mo}$, $GMPI_{As-Sb}$, and $GMPI_{Pb-Zn}$ respectively.

3.3. Mapping multi-element geochemical signatures

In order to map the geochemical signatures, a suitable unit cell size must be selected (Carranza, 2009; Zuo, 2012). An appropriate cell size can be defined as $\sqrt{\frac{A}{n}} \times 0.05$ (Hengl, 2006), where A is the total area of a map and n is the total number of observations. Here, A is approximately 6×10^8 m^2, and n is 174, and the cell size would be 93 m. Hence, we used a pixel size of 90 m × 90 m for all the raster maps in this study.

For mapping geochemical anomalies we used two methods, contour mapping as the continuous method (e.g., Howarth, 1983) and SCB as the discrete model (e.g., Carranza and Hale, 1997), for comparison purposes. Ordinary inverse distance weighting method (IDW) was used as an interpolation approach for modeling geochemical signatures in contour maps. For this, the transformed values of geochemical signatures, $GMPI_{Au-Ag-Cu-Mo}$ (Fig. 3), $GMPI_{Pb-Zn}$ (Fig. 4) and $GMPI_{As-Sb}$ (Fig. 5) were mapped. On the other hand, because materials of stream sediment samples are representative of their upstream composition (Spadoni, 2006; Carranza, 2008), the SCB model (Bonham-Carter, 1994; Bonham-Carter and Goodfellow, 1984, 1986; Carranza and Hale, 1997; Moon, 1999; Spadoni et al., 2004; Carranza, 2008; Carranza, 2010b), SCB was used to model the geochemical signatures, i.e., $GMPI_{Au-Ag-Cu-Mo}$, $GMPI_{Pb-Zn}$, and $GMPI_{As-Sb}$, respectively in Figs. 6, 7, 8.

3.4. Recognizing efficient geochemical signatures

For recognizing efficient multi-element geochemical signatures we used the location of known mineral occurrences as testing points (e.g., Agterberg and Bonham-Carter, 2005; Porwal et al., 2003, 2004, 2006). For this, we used P-A plots (Yousefi and Carranza, 2015a, 2015b), normalized density (Mihalasky and Bonham-Carter, 2001), and success rate curves (e.g., Agterberg and Bonham-Carter, 2005; Carranza and Laborte, 2015c).

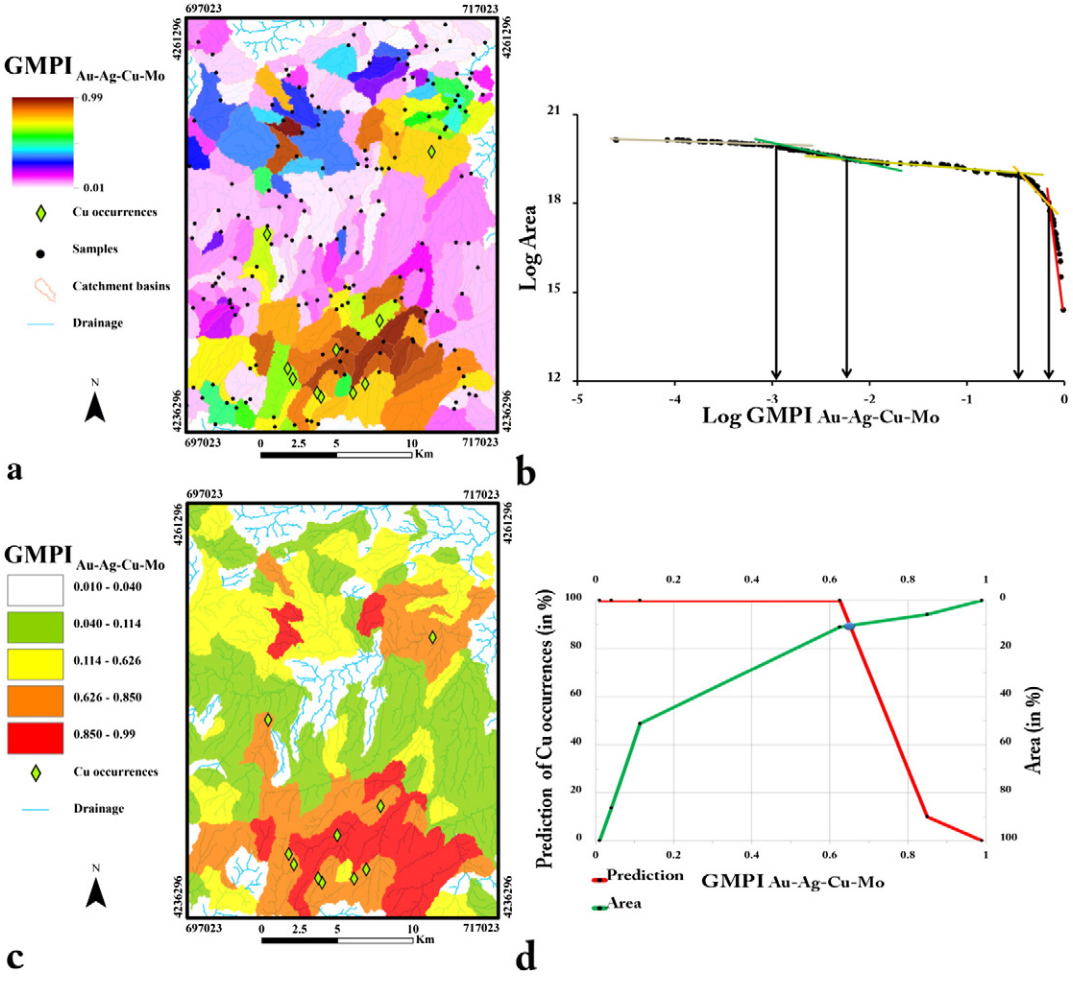

Fig. 6. SCB model for the $GMPI_{Au-Ag-Cu-Mo}$ values (a), C-A fractal model (b), classified map (c), and P-A plot (d).

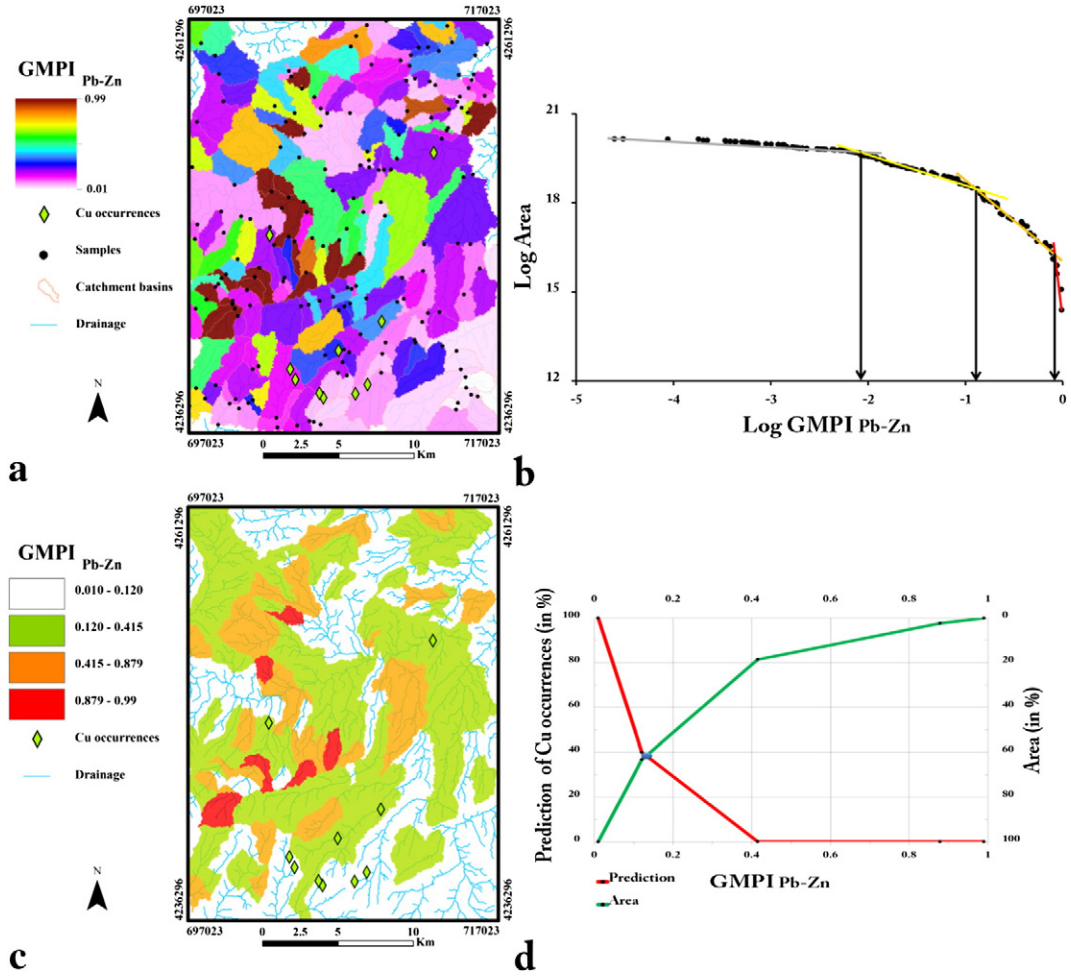

Fig. 7. SCB model for the $GMPI_{Pb-Zn}$ values (a), C-A fractal model (b), classified map (c), and P-A plot (d).

For generation of P-A plots and success rate curves, the values of geochemical signatures should be discretized (Yousefi and Carranza, 2015a; Agterberg and Bonham-Carter, 2005). In this regard, fractal methods (e.g., Mandelbrot, 1983; Cheng et al., 1994; Afzal et al., 2010; Li et al., 2003; Cheng et al., 2000; Cheng, 2007) can be employed for discretization and classification of geochemical signatures. The concentration-area (C-A) fractal model (Cheng et al., 1994) is applicable for both SCB (e.g., Carranza, 2008, 2011) and contour maps (e.g., Cheng et al., 1994; Carranza, 2008; Zuo, 2011a; Zuo et al., 2013). Accordingly, we used the C-A model (Figs. 3b–8b) in order to classify geochemical populations in both SCB models and contour maps. Based on the classified maps (Figs. 3c–8c), occupied area of each class, and the location of the known mineral occurrences, P-A plots were then generated for each of the geochemical signature layers (Figs. 3d–8d). P-A plot is drawn by plotting the prediction rate and the occupied area of each class of geochemical signature, versus their corresponding threshold values (Yousefi and Carranza, 2015b). Then, according to Yousefi and Carranza (2015a, 2015b), the parameters of the intersection point of the two curves (i.e., prediction rate and occupied area) in the P-A plots were extracted and used to calculate normalized density, N_d, and weight of the geochemical evidence layers, W_e, (Table 2). N_d is calculated as the prediction rate of a geochemical evidence layer divided by its corresponding occupied area extracted from the intersection point of the P-A plot, and W_e is calculated by taking the ln of N_d (Mihalasky and Bonham-Carter, 2001, Yousefi and Carranza, 2015b). The details for making the P-A plot and calculating N_d and W_e of an evidence layer are found in Yousefi and Carranza (2015b).

In addition to the P-A plot and normalized density, we used a modified success rate curve with a gauge line ($N_d = 1$) proposed by Parsa et al. (2016) for further evaluation of geochemical signatures. The success rate curve (Chung and Fabri, 2003; Agterberg and Bonham-Carter, 2005) is drawn by plotting the portion of mineral occurrences predicted correctly, P_o, in vertical axis versus the portion of the study area classified as prospective, P_a, in horizontal axis (e.g., Carranza and Laborte, 2015c). We used the threshold values derived by C-A models (Figs. 3b–8b) for generation of success rate curves (Fig. 9). In the modified success rate curve the diagonal line, which represents $N_d = 1$ and $W_e = 0$, is a criterion for evaluation the relative importance of geochemical signature maps (Parsa et al., 2016). The N_d close to 1 for a class of prospectivity, here a class of geochemical anomaly, indicates that the class consists of randomly selected pixels and hence is an unsupportive prediction class (Chung and Fabri, 2003). Thus, the diagonal line on the plot of the success rate curve is a gauge line for separating efficient and inefficient geochemical signatures of the deposit-type sought (Parsa et al., 2016). In this regard, if the success rate curve of a geochemical evidence layer appears under the gauge line, it represents negative spatial association of the evidence layer with the mineralization and thus, the geochemical signature is not a good indicator of the deposit-type sought. On the other hand if the success rate curve of a geochemical evidence layer appears above the gauge line, it represents positive spatial association of the evidence layer with the

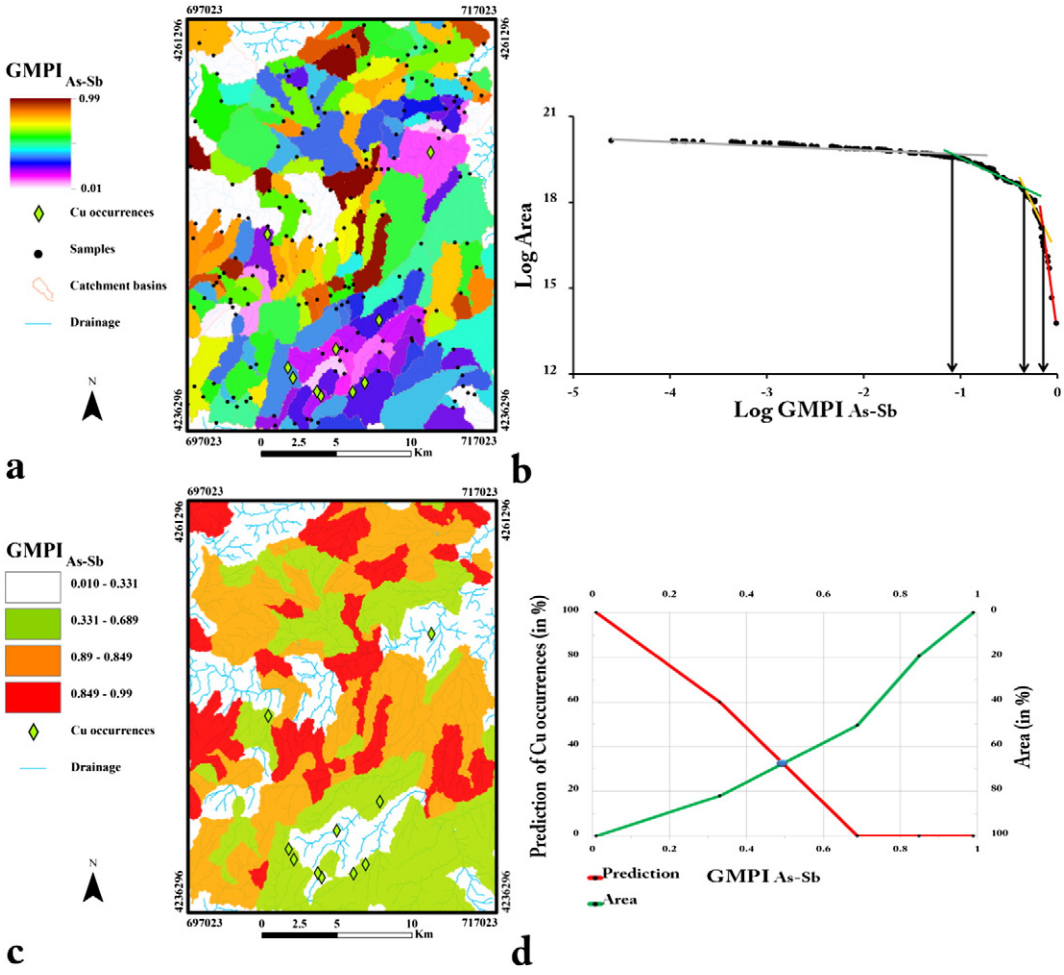

Fig. 8. SCB model for the $GMPI_{As-Sb}$ values (a), C-A fractal model (b), classified map (c), and P-A plot (d).

mineralization and thus, the geochemical signature is an efficient indicator of the deposit-type sought. This is because a value of $N_d > 1$ ($W_e > 0$) for a map of geochemical signatures, indicates a positive association of the signature with the mineralization of the type sought, while a value of $N_d < 1$ ($W_e < 0$) for a map of geochemical signatures, indicates a negative association of the signature with the mineralization of the type sought (Mihalasky and Bonham-Carter, 2001, Yousefi and Carranza, 2015b). In addition, if the success rate curve of a certain geochemical evidence layer appears in higher above the gauge line in comparison with the success rate curves of other geochemical evidence layers, it represents better spatial association with the mineralization (Parsa et al., 2016).

For the study area in this paper, the value of W_e for $GMPI_{Au-Ag-Cu-Mo}$ in the SCB model and contour map (Figs. 3, 6) is >0, 2.19 and 1.81 respectively (Table 2). The success rate curve for this geochemical signature ($GMPI_{Au-Ag-Cu-Mo}$ in SCB model and contour map) (Fig. 9) appears above the gauge line. Thus, these two models are significant indicators of the deposit-type sought. The values of W_e for $GMPI_{Pb-Zn}$ and $GMPI_{As-Sb}$ in SCB models (Figs. 4, 5) and contour maps (Figs. 7, 8) are <0 (Table 2). The success rate curves for these geochemical signatures appear under the diagonal line (Fig. 9). So, these two signatures (modeled as four maps in Figs. 4, 5, 7, 8) are inefficient indicators of the deposit-type sought in the study area, and as Yousefi and Carranza (2015b) demonstrated such indicators should be excluded from the integration stages in MPM.

Table 2
Prediction rate (P_r), occupied area (O_a), normalize density (N_d) and the weight (W_e) of different geochemical signature layers. Values in bold represent efficient indicators.

Evidential layer	P_r (in %)	O_a (in %)	N_d	W_e
SCB model of $GMPI_{Au-Cu-Mo}$	90	10	**9**	**2.19**
Interpolated values of $GMPI_{Au-Cu-Mo}$	86	14	**6.14**	**1.81**
SCB model of $GMPI_{As-Sb}$	31	69	0.44	−0.80
Interpolated values of $GMPI_{As-Sb}$	23	77	0.29	−1.20
SCB model of $GMPI_{Pb-Zn}$	39	61	0.63	−0.44
Interpolated values of $GMPI_{Pb-Zn}$	38	62	0.61	−0.48

3.5. Exploring the effect of mapping methods of geochemical signatures in MPM

According to the analyses explained above, the $GMPI_{Au-Ag-Cu-Mo}$ is the most effective geochemical signature of the deposit-type sought in the study area, and there are two different models for this geochemical signature, contour map and SCB. For exploring the effect of using a stronger multi-element geochemical signature layer to MPM, we generated two individual prospectivity models by integration of the contour map and SCB model individually with another geological evidence layer for comparison purpose. If a set of efficient evidential layers are combined with each other, more reliable target areas are generated for the deposit-type sought (Carranza, 2008; Yousefi and Carranza, 2015a, 2015b).

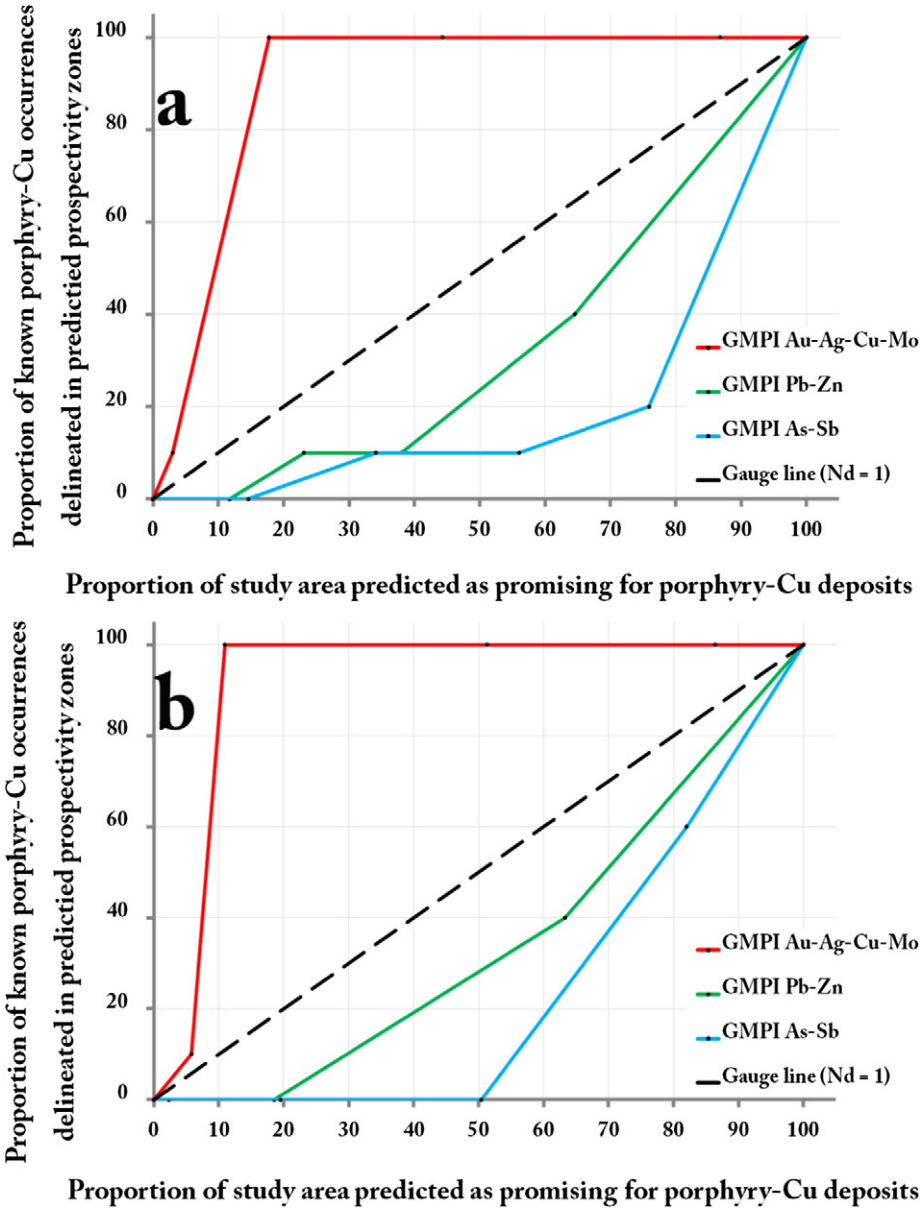

Fig. 9. Success rate curves of the GMPIs for interpolated maps (a) and SCB models (b).

The derived geochemical signature layer, $GMPI_{Au-Ag-Cu-Mo}$, is, in fact, a fuzzy geochemical evidence layer, so we used a fuzzy fault density (FD) map as another evidential layer in Fuzzy logic MPM (e.g., Porwal et al., 2003). The FD map was selected because intersections of faults are typically favorable places for focusing hydrothermal fluids and therefore for the formation of porphyry Cu deposits (e.g., Carranza and Hale, 2002; Pirajno, 2010; Chen et al., 2011). For generating the fuzzy FD layer, the total length of faults per pixel was calculated. Then we used Eq. (1) of Yousefi and Carranza (2015a) in order to transform FD values into a [0,1] range, fuzzy score (Fig. 10a). Then for evaluating the efficiency of the evidence layer of FD in predicting mineral deposits, the C-A fractal model (Fig. 10b) was used to classify the transformed FD values (Fig. 10c). In the next stage, like other evidence layers in this study, the corresponding P-A plot (Fig. 10d) was drawn. Considering the parameters of the intersection point of the prediction and area curves in Fig. 10d, the weight for FD evidence layer, W_e, was obtained as 1.90. Therefore like $GMPI_{Au-Ag-Cu-Mo}$, FD evidence layer is another efficient indicator for the deposit-type sought. Thus, the two models of efficient geochemical signatures (i.e., $GMPI_{Au-Ag-Cu-Mo}$), SCB model (Fig. 6) and the map of interpolated $GMPI_{Au-Ag-Cu-Mo}$ values (Fig. 3) were individually integrated with the FD evidence layer by using the fuzzy gamma (=0.9) operator (e.g., Porwal et al., 2003; Yousefi et al., 2013) to generate two prospectivity models (Figs. 11a, 12a).

To evaluate and compare the generated prospectivity models we used P-A plot. For this, the C-A fractal model (Fig. 11b), classified map (Fig. 11c), and P-A plot (11d) were prepared for mineral prospectivity model in Fig. 11a, generated by integration of interpolated values of $GMPI_{Au-Ag-Cu-Mo}$ and evidence layer of fault density. Likewise, the C-A fractal model (Fig. 12b), classified map (Fig. 12c), and P-A plot (12d) were prepared for mineral prospectivity model in Fig. 11a, generated by integration of SCB model of $GMPI_{Au-Ag-Cu-Mo}$ and evidence layer of fault density. Then, based on the extracted parameters of the intersection points in the P-A plot, N_d and W_e were calculated for the two prospectivity models (Table 3) for the comparison purpose. Fig. 13 shows success rate curves for the two prospectivity models as well. Based on Fig. 13, despite the success rate curves for the two

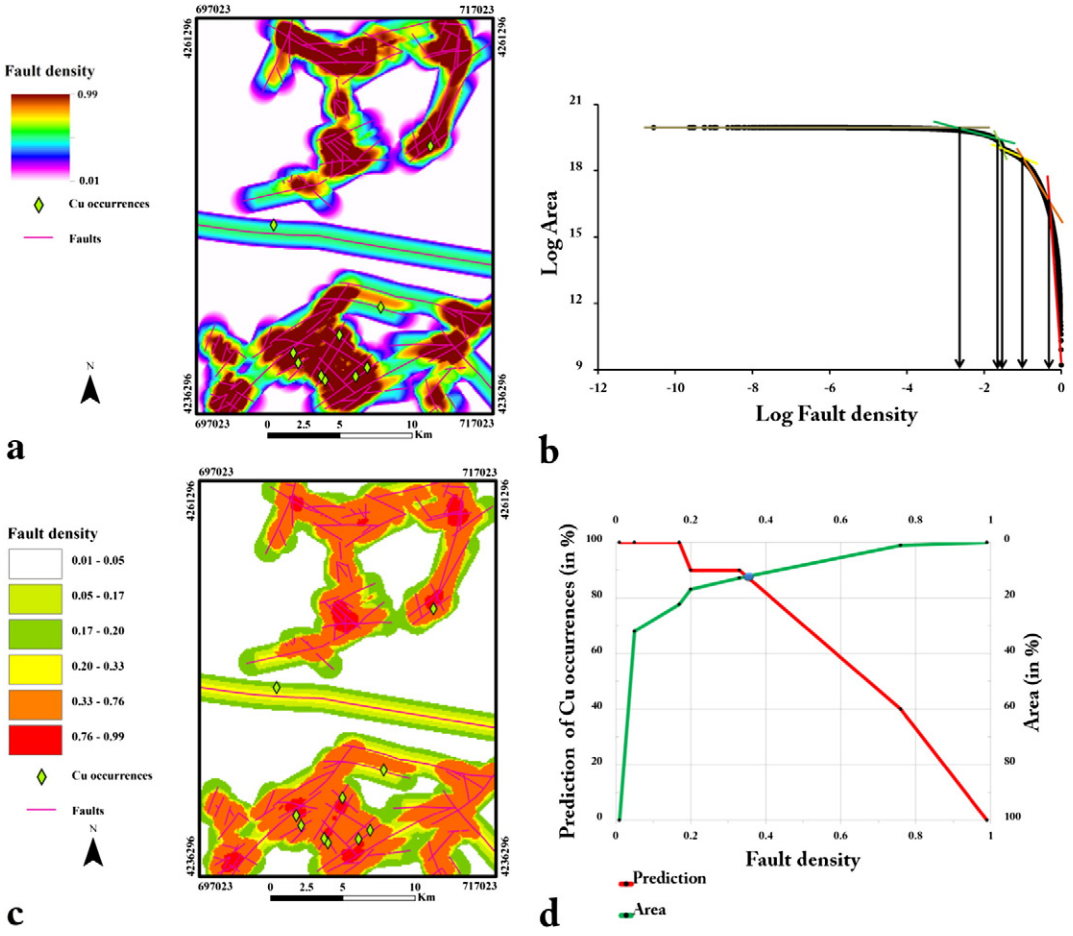

Fig. 10. Distribution map of transformed values of fault density (a), C-A fractal model (b), classified map (c), and P-A plot (d).

prospectivity models appear on the top of the diagonal line and so both of the models have positive spatial association with the mineral deposit of the type sought, the success rate curve for the prospectivity model generated by integration of SCB model of the $GMPI_{Au-Ag-Cu-Mo}$ values with the fuzzy FD layer appears even higher above the gauge line. Thus the latter is the better model to be used for further exploration. Such results are obtained from P-A plots and Table 3. The prediction rate of the fuzzy mineral prospectivity map generated by integration of interpolated $GMPI_{Au-Ag-Cu-Mo}$ values with a fuzzy FD layer is 86% (Fig. 11d and Table 3), while the prediction rate of the fuzzy mineral prospectivity map generated by integration of the SCB model of the $GMPI_{Au-Ag-Cu-Mo}$ values with a fuzzy FD layer is 92% (Fig. 12d and Table 3). Accordingly, N_d and W_e for the prospectivity model generated by integration of the FD evidence layer with the SCB model of $GMPI_{Au-Ag-Cu-Mo}$ values are greater than those of the prospectivity model generated by integration of FD evidence layer with interpolated map of $GMPI_{Au-Ag-Cu-Mo}$ values,11.5 > 6.14 and 2.44 > 1.81 (Figs. 11d, 12d and Table 3).

4. Discussion

In this paper, exploring the effects of mapping methods of geochemical anomalies in prediction of mineral deposits and delimiting the study area show that SCB model is more efficient than contour maps for target generation, especially for MPM. This is due to the smoothing effect of ordinary moving average contour mapping methods (e.g., IDW) that adversely affects the modeling of geochemical anomalies of stream sediment data (Zuo, 2011b) by neglecting locally high values. In addition, stream sediment data are irregularly sampled, and thus contour mapping of geochemical anomalies is not the best choice for modeling the spatial distribution of stream sediment data.

There are various factors that affect dispersion patterns of geochemical elements in different areas (Spadoni, 2006; Cheng, 2007; Yousefi et al., 2013). Thus, it is important to analyze and recognize significant geochemical signatures representing the deposit-type sought in a study area for further exploration (e.g., Andrada de Palomera et al., 2012; Yousefi and Nykänen, 2015; Parsa et al., 2016). In this regard, multi-element associations of Zn–Pb, As–Sb, and Au–Ag–Cu–Mo have been used as indicators for prospecting porphyry-Cu deposits in different areas (Cooke et al., 2005; Weixuan et al., 2007; Yang et al., 2009; Yousefi et al., 2012), but in the study area the Zn–Pb and As–Sb associations have not shown positive spatial association with the deposit-type sought, and so, they are not significant geochemical signatures for the deposit. As demonstrated in this paper, the Au–Ag–Cu–Mo association is a strong geochemical signature for the deposit-type sought.

Recognizing geochemical anomalies and modeling their spatial associations with particular geological features are critical aspects for mineral exploration and understanding ore geometry (Ziaii et al., 2011; Wang et al., 2013). Considering the results of the second stage of RFA (Table 1), the first factor shows Au–Ag–Cu–Mo enrichment and Pb–Zn depletion (cf. Filzmoser et al., 2009b). This shows that these two groups of elements (Au–Ag–Cu–Mo and Pb–Zn) have different dispersion patterns (Figs. 3, 4, 6, 7). In the study area of this paper, geochemical signatures of $GMPI_{Pb-Zn}$ (Figs. 4, 7) and $GMPI_{As-Sb}$ (Figs. 5, 8) show distal halos from the outcropping mineralized zones. On the other hand,

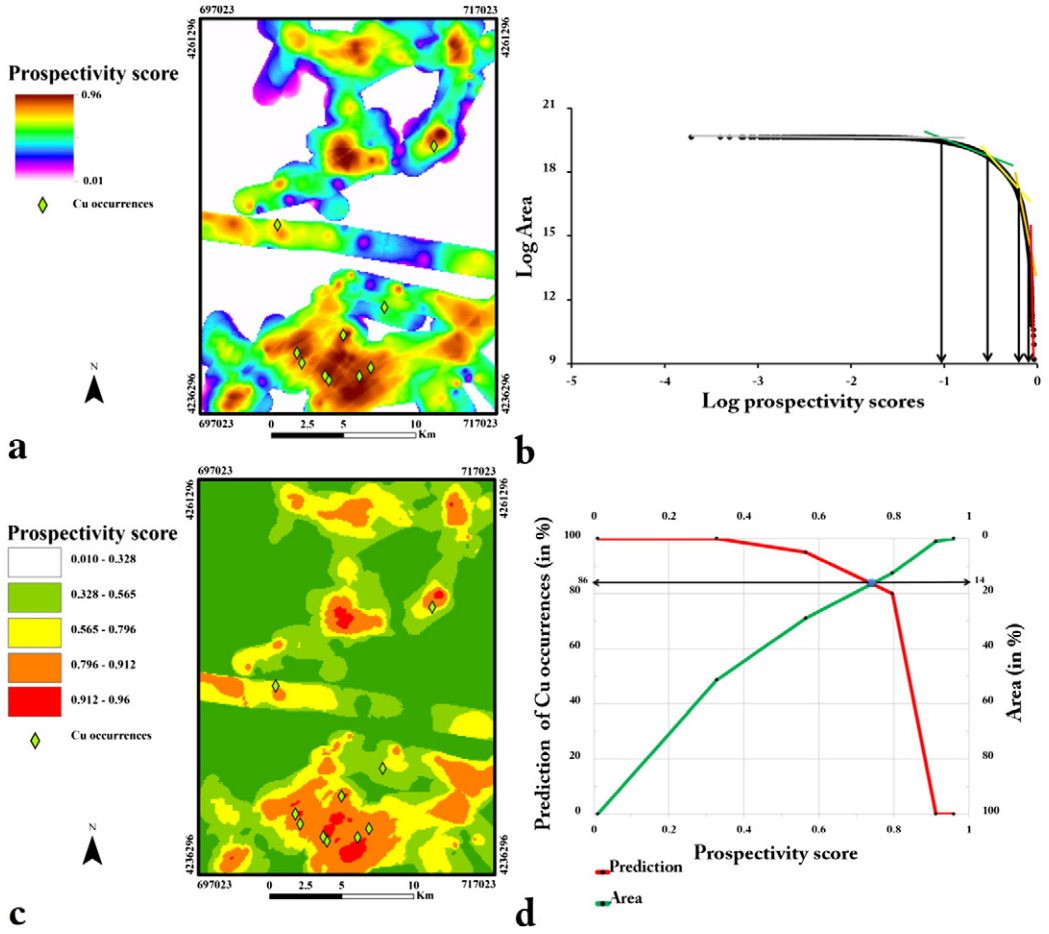

Fig. 11. Mineral prospectivity model generated by integration of interpolated values of $GMPI_{Au–Ag–Cu–Mo}$ and evidence layer of fault density (a), C-A fractal model (b), classified map of the mineral prospectivity model (c), and P-A plot (d).

geochemical signature of $GMPI_{Au–Ag–Cu–Mo}$ shows proximal halos to the outcropping mineralized zones (Figs. 3, 6). This surficial zoning pattern is analogous to those reported from several known porphyry-Cu systems (e.g., Meinert, 2000; Sillitoe, 2010), and thus, the delimited targets in the study area should be evaluated for further explorations.

The efficiency of mineral prospectivity models and the reliability of delimited target areas could be enhanced by recognizing of efficient and inefficient indicators and exclusion of inefficient indicators from the process of target generation in MPM (Yousefi and Carranza, 2015a, 2015b; Parsa et al., 2016). In this regard, receiver operating characteristics (ROC) analysis (Swets, 1988) and success rate curves (Chung and Fabbri, 2003; Agterberg and Bonham-Carter, 2005) could be employed to assess the ability of evidence layers or geochemical signatures in predicting mineral deposits (e.g., Carranza, 2008; Nykänen et al., 2014; Andrada de Palomera et al., 2014; Carranza and Laborte, 2015c). In this paper we used P-A plot (Yousefi and Carranza, 2015b) in conjunction with a success rate curve with a gauge line ($N_d = 1$ and $W_e = 0$) (Parsa et al., 2016) to evaluate different geochemical signatures, and consequently to discriminate efficient and inefficient signatures of the deposit-type sought.

5. Concluding remarks

1- Recognizing significant multi-element geochemical signatures of a mineral deposit of the type sought in an area is important because despite the presence of generally common indicator elements that are genetically related to the mineralization, the dispersion pattern of indicator elements in different areas can differ. Thus, certain indicator elements (or multi-element signatures) cannot be used efficiently in different areas because the dispersion patterns of indicator elements are affected by characteristics of the study area.

2- Mineral prospectivity models are affected by applied methods for geochemical anomaly modeling. In this regard, based on the results of this paper sample catchment basin modeling of geochemical anomalies result in more reliable target areas for further exploration in comparison with contour maps. Sample catchment basin modeling increases the prediction rate of mineral deposits as well.

3- Prediction-area (P-A) plot and the plot of success-rate curve with a gauge line ($N_d = 1$) are powerful tools to recognize significant multi-element geochemical signatures. They can be applied efficiently to evaluate and rank maps of geochemical signatures. Thus, effective and ineffective indicators of geochemical signatures for exploration of a certain deposit-type are recognized.

Acknowledgment

The authors thank Prof. John Carranza, Associate Editor, and two anonymous reviewers for their constructive comments.

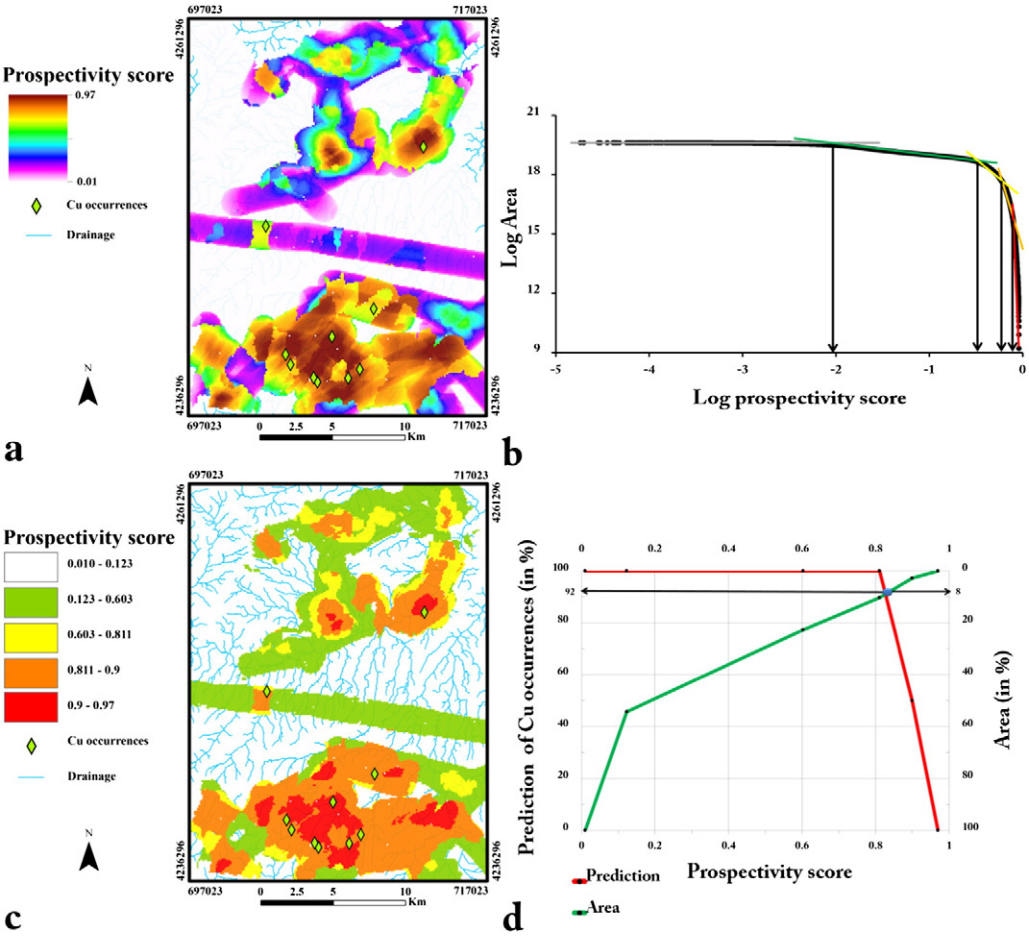

Fig. 12. Mineral prospectivity model generated by integration of SCB model of $GMPI_{Au–Ag–Cu–Mo}$ and evidence layer of fault density (a), C-A fractal model (b), classified map of the mineral prospectivity model (c), and P-A plot (d).

Table 3
Prediction rate (P_r), occupied area (O_a), normalize density (N_d) and the weight (W_e) of prospectivity models generated using two different geochemical evidence layers.

Prospectivity model	P_r (in %)	O_a (in %)	N_d	W_e
Generated using interpolated geochemical values	86	14	6.14	1.81
Generated using SCB model of geochemical values	92	8	11.5	2.44

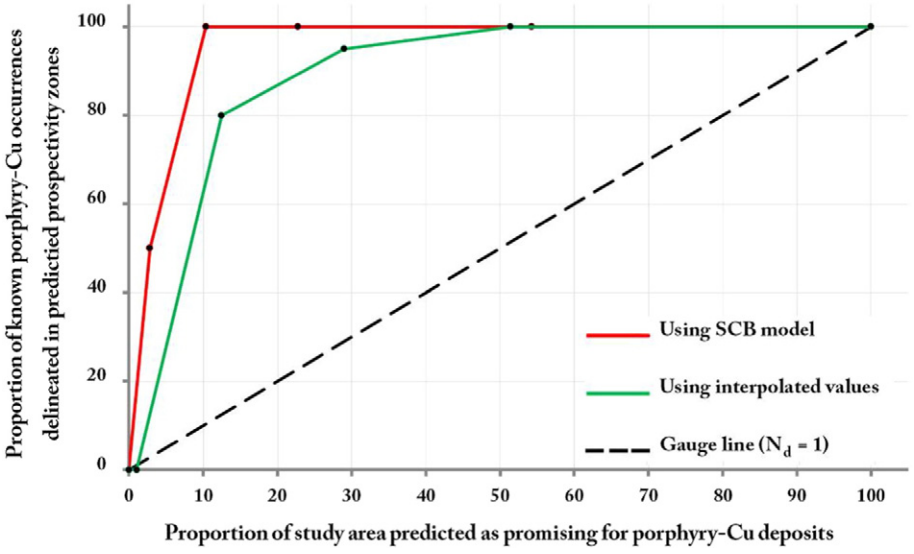

Fig. 13. Success rate curves of prospectivity models generated using two different types of geochemical evidence layers.

References

Afzal, P., Khakzad, A., Moarefvand, P., Rashidnejad Omran, N., Esfandiari, B., Fadakar Alghalandis, Y., 2010. Geochemical anomaly separation by multifractal modeling in Kahang (Gor Gor) porphyry system, Central Iran. J. Geochem. Explor. 104, 34–46.

Agterberg, F.P., 1992. Combining indicator patterns in weights of evidence modeling for resource evaluation. Nat. Resour. Res. 1, 39–50.

Agterberg, F.P., Bonham-Carter, G.F., 2005. Measuring the performance of mineral-potential maps. Nat. Resour. Res. 14, 1–17.

Aitchison, J., 1986. The Statistical Analysis of Compositional Data. Chapman and Hall, London 416 p.

Aitchison, J., Egozcue, J.J., 2005. Compositional data analysis: where are we and where should we be heading? Math. Geol. 37, 829–850.

Aitchison, J., Greenacre, M., 2002. Biplots of compositional data. Appl. Stat. 51, 375–392.

Andrada de Palomera, P., Van Ruitenbeek, F.J., Van der Meer, F.D., Fernández, R., 2012. Geochemical indicators of gold-rich zones in the La Josefina epithermal deposit, Deseado Massif, Argentina. Ore Geol. Rev. 45, 61–80.

Andrada de Palomera, P., Van Ruitenbeek, F.J., Carranza, E.J.M., 2014. Prospectivity for epithermal gold–silver deposits in the Deseado Massif, Argentina. Ore Geol. Rev. http://dx.doi.org/10.1016/j.oregeorev.2014.12.007.

Ayati, F., Yazuf, F., Asadi, H., Richards, J.P., Jourdane, F., 2013. Petrology and geochemistry of cal-alkaline volcanic and subvolcanic rocks, Dali porphyry copper-gold deposit, Markazi province, Iran. Int. Geol. Rev. 55, 158–184.

Babaie, H.A., Ghazi, A.M., Babaei, A., La Tour, T.E., Hassanipak, A.A., 2001. Geochemistry of arc volcanic rocks of the Zagros Crush Zone, Neyriz, Iran. J. Asian Earth Sci. 19, 61–76.

Bai, J., Porwal, A., Hart, C., Ford, A., Yu, L., 2010. Mapping geochemical singularity using multifractal analysis: application to anomaly definition on stream sediments data from Funin Sheet, Yunnan, China. J. Geochem. Explor. 104, 1–11.

Berberian, M., King, G.C., 1981. Towards a paleogeography and tectonic evolution of Iran. Can. J. Earth Sci. 18, 210–265.

Berberian, F., Muir, I.D., Pankhurst, R.J., Berberian, M., 1982. Late Cretaceous and early Miocene Andean-type plutonic activity in northern Makran and Central Iran. J. Geol. Soc. 139, 605–614.

Billa, M., Cassard, D., Lips, A.L.W., Bouchot, V., Tourlière, B., Stein, G., Guillou-Frottier, L., 2004. Predicting gold-rich epithermal and porphyry systems in the central Andes with a continental-scale metallogenic GIS. Ore Geol. Rev. 25, 39–67.

Bonham-Carter, G.F., 1994. Geographic Information Systems for Geoscientists: Modelling With GIS. Pergamon, Oxford.

Bonham-Carter, G.F., Goodfellow, W.D., 1984. Autocorrelation structure of stream-sediment geochemical data: interpretation of Zn and Pb anomalies, Nahanni River area, Yukon-Northwest Territories, Canada. In: Verly, G., David, M., Journel, A.G., Marechal, A. (Eds.), Geostatistics for Natural Resources Characterization Part 2, pp. 817–829.

Bonham-Carter, G.F., Goodfellow, W.D., 1986. Background corrections to stream geochemical data using digitized drainage and geological maps: application to Selwyn Basin, Yuk on and Northwest Territories. J. Geochem. Explor. 25, 139–155.

Bonham-Carter, G.F., Rogers, P.J., Ellwood, D.J., 1987. Catchment basin analysis applied to surficial geochemical data, Cobequid Highlands, Nova Scotia. J. Geochem. Explor. 29, 259–278.

Bonham-Carter, G.F., Agterberg, F.P., Wright, D.F., 1988. Integration of geological datasets for gold exploration Nova Scotia. Photogramm. Eng. Rem. S. 54, 1585–1592.

Borovec, Z., 1996. Evaluation of the concentrations of trace elements in stream sediments by factor and cluster analysis and the sequential extraction procedure. Sci. Total Environ. 177, 237–250.

Buccianti, A., 2015. The FOREGS repository: modelling variability in stream water on a continental scale revising classical diagrams from CoDA (compositional data analysis) perspective. J. Geochem. Explor. 154, 94–104.

Buccianti, A., Grunsky, E., 2014. Compositional data analysis in geochemistry: are we sure to see what really occurs during natural processes? J. Geochem. Explor. 141, 1–5.

Buccianti, A., Lima, A., Albanese, S., Cannatelli, C., Esposito, R., De vivo, B., 2015. Exploring topsoil geochemistry from the CoDA (Compositional Data Analysis) perspective: the multi-element data archive of the Campania Region (Southern Italy). J. Geochem. Explor. 159, 302–316.

Carranza, E.J.M., 2004. Usefulness of stream order to detect stream sediment geochemical anomalies. Geochem.: Explor., Environ., Anal. 4, 341–352.

Carranza, E.J.M., 2008. Geochemical Anomaly and Mineral Prospectivity Mapping in GIS. Handbook of Exploration and Environmental Geochemistry 11. Elsevier, Amsterdam.

Carranza, E.J.M., 2009. Objective selection of suitable unit cell size in data-driven modeling of mineral prospectivity. Comput. Geosci. 35, 2032–2046.

Carranza, E.J.M., 2010a. Catchment basin modeling of stream sediment anomalies revisited: incorporation of EDA and fractal analysis. Geochem.: Explor., Environ., Anal. 10, 356–381.

Carranza, E.J.M., 2010b. Mapping of anomalies in continuous and discrete fields of stream sediment geochemical landscapes. Geochem.: Explor., Environ., Anal. 10, 171–187.

Carranza, E.J.M., 2011. Analysis and mapping of geochemical anomalies using logratio-transformed stream sediment data with censored values. J. Geochem. Explor. 110, 167–185.

Carranza, E.J.M., 2015. Data-driven evidential belief modeling of mineral potential using few prospects and evidence with missing values. Nat. Resour. Res. 24, 291–304.

Carranza, E.J.M., Hale, M., 1997. A catchment basin approach to the analysis of geochemical-geological data from Albay Province, Philippines. J. Geochem. Explor. 60, 157–171.

Carranza, E.J.M., Hale, M., 2002. Where are porphyry copper deposits spatially localized? A case study in Benguet Province, Philippines. Nat. Resour. Res. 11, 45–59.

Carranza, E.J.M., Laborte, A.G., 2015a. Data-driven predictive mapping of gold prospectivity, Baguio district, Philippines: application of Random Forests algorithm. Ore Geol. Rev. 71, 777–787.

Carranza, E.J.M., Laborte, A.G., 2015b. Data-driven predictive modeling of mineral prospectivity using random forests: a case study in Catanduanes Island (Philippines). Nat. Resour. Res. http://dx.doi.org/10.1007/s11053-015-9268-x.

Carranza, E.J.M., Laborte, A.G., 2015c. Random forest predictivity modeling of mineral prospectivity with small number of prospects and data with missing values in Abra (Philipines). Comput. Geosci. 74, 60–70.

Chandrajith, R., Dissanayake, C.B., Tobschall, H.J., 2001. Application of multi-element relationships in stream sediments to mineral exploration: a case study of Walawe Ganga Basin, Sri Lanka. Appl. Geochem. 16, 339–350.

Chen, Z., Zhang, L., Wan, B., Wu, H., Cleven, N., 2011. Geochronology and geochemistry of the Wunugetushan porphyry Cu–Mo deposit in NE china, and their geological significance. Ore Geol. Rev. 43, 92–105.

Cheng, Q., 2007. Mapping singularities with stream sediment geochemical data for prediction of undiscovered mineral deposits in Gejiu, Yunnan Province, China. Ore Geol. Rev. 321, 314–324.

Cheng, Q., Agterberg, F.P., Ballantyne, S.B., 1994. The separation of geochemical anomalies from background by fractal methods. J. Geochem. Explor. 54, 109–130.

Cheng, Q., Xu, Y., Grunsky, E., 2000. Integrated spatial and spectrum method for geochemical anomaly separation. Nat. Resour. Res. 91, 43–52.

Chung, C.J.F., Fabrri, A.G., 2003. Validation of spatial prediction models for landslide hazard mapping. Nat. Hazards 30, 451–472.

Cooke, D.R., Hollings, P., Walshe, J.L., 2005. Giant porphyry deposits: characteristics, distribution, and tectonic controls. Econ. Geol. 100, 801–818.

R Development Core Team, 2008. R: A Language and Environment for Statistical Computing. Vienna http://www.r-project.org.

Egozcue, J.J., Pawlowsky-Glahn, V., Mateu-Figueras, G., Barceló-Vidal, C., 2003. Isometric logratio transformations for compositional data analysis. Math. Geol. 35, 279–300.

El-Makky, A.M., 2011. Statistical analyses of La, Ce, Nd, Y, Nb, Ti, P, and Zr in bedrocks and their significance in geochemical exploration at the Um Garayat Gold Mine Area, Eastern Desert, Egypt. Nat. Resour. Res. 20, 157–176.

El-Makky, A.M., Sediek, K.N., 2012. Stream sediments geochemical exploration in the northwestern part of Wadi Allaqi Area, South Eastern Desert, Egypt. Nat. Resour. Res. 21, 95–115.

Filzmoser, P., Hron, K., Reimann, C., 2009a. Principal component analysis for compositional data with outliers. Environmetrics 20, 621–632.

Filzmoser, P., Hron, K., Reimann, C., Garrett, R., 2009b. Robust factor analysis for compositional data. Comput. Geosci. 35, 1854–1861.

Filzmoser, P., Hron, K., Reimann, C., 2009c. Univariate statistical analysis of environmental (compositional) data: problems and possibilities. Sci. Total Environ. 407, 6100–6108.

Ford, A., Blenkinsop, T.G., 2008. Evaluating geological complexity and complexity gradients as controls on copper mineralization, Mt Isa Inlier. Aust. J. Earth Sci. 55, 13–23.

Gholami, R., Moradzadeh, A., Yousefi, M., 2012. Assessing the performance of independent component analysis in remote sensing data processing. J. Indian Soc. Remote Sens. 40, 577–588.

Ghorbani, M., 2013. The Economic Geology of Iran: Mineral Deposits and Natural Resources. Springer Science and Business Media.

Grunsky, E.C., 2010. The interpretation of geochemical survey data. Geochem.: Explor., Environ., Anal. 10, 27–74.

Harris, D., Zurcher, L., Stanley, M., Marlow, J., Pan, G., 2003. A comparative analysis of favorability mappings by weights of evidence, probabilistic neural networks, discriminant analysis, and logistic regression. Nat. Resour. Res. 12, 241–255.

Hawkes, H.E., 1976. The downstream dilution of stream sediment anomalies. J. Geochem. Explor. 6, 345–358.

He, J., Yao, S., Zhang, Z., You, G., 2013. Complexity and productivity differentiation models of metallogenic indicator elements in rocks and supergene media around Daijiazhuang Pb–Zn deposit in Dangchang County, Gansu Province. Nat. Resour. Res. 22, 19–36.

He, F.P., Wang, Z., Fang, C., Wang, L., Geng, X., 2014. Identification and assessment of Sn-polymetallic prospects in the Gejiu western district, Yunnan (China). J. Geochem. Explor. 145, 106–113.

Helvoort, P.J., Filzmoser, P., Van Gaans, P.F., 2005. Sequential factor analysis as a new approach to multivariate analysis of heterogeneous geochemical datasets: an application to a bulk chemical characterization of fluvial deposits (Rhine–Meuse delta, The Netherlands). Appl. Geochem. 20, 2233–2251.

Hengl, T., 2006. Finding the right pixel size. Comput. Geosci. 32, 1283–1298.

Howarth, R.J., 1983. Mapping. In: Howarth, R.J. (Ed.), Statistics and Data Analysis in Geochemical Prospecting, Handbook of Exploration Geochemistry 2. Elsevier, Amsterdam, pp. 111–205.

Kaiser, H.F., 1958. The varimax criteria for analytical rotation in factor analysis. Psychometrika 23, 187–200.

Kumru, M.N., Bakac, M., 2003. R-mode factor analysis applied to the distribution of elements in soils from the Aydın basin, Turkey. J. Geochem. Explor. 77, 81–91.

Levitan, D.M., Zipper, C.E., Donovan, P., Schreiber, M.E., Seal, R.R., Engle, M.A., Chermak, J.A., Bodnar, R.J., Johnson, D.K., Aylor, J.G., 2015. Statistical analysis of soil geochemical data to identify pathfinders associated with mineral deposits: an example from Coles Hill Uranium deposit, Virginia, USA. J. Geochem. Explor. 154, 238–251.

Li, C., Ma, T., Shi, J., 2003. Application of a fractal method relating concentrations and distances for separation of geochemical anomalies from background. J. Geochem. Explor. 77, 167–175.

Liu, Y., Cheng, Q., Xia, Q., Wang, X., 2014. Mineral potential mapping for tungsten polymetallic deposits in the Nanling metallogenic belt, South China. J. Earth Sci. 25, 689–700.

Lusty, P.A.J., Schieb, C., Gunn, A.G., Walker, A.S.D., 2012. Reconnaissance-scale prospectivity analysis for gold mineralisation in the Southern Uplands-Down-Longford Terrane, Northern Ireland. Nat. Resour. Res. 21, 359–382.
Maghsoudi, A., Yazdi, M., Mehrpartou, M., Vosoughi, M., Younesi, S., 2014. Porphyry Cu–Au mineralization in the Mirkuh Ali Mirza magmatic complex, NW Iran. J. Asian Earth Sci. 79, 932–941.
Mahdavi, M.A., Amini Fazl, A., 1988. Geological Map of Iran 1: 100,000 Series, Ahar. Geological Survey of Iran, Tehran.
Mandelbrot, B.B., 1983. The Fractal Geometry of Nature. W.H. Freeman, San Francisco, CA. Updated and Augmented Edition.
Meinert, L.D., 2000. Gold in skarns related to epizonal intrusions. Rev. Econ. Geol. 13, 347–375.
Mihalasky, M.J., Bonham-Carter, G.F., 2001. Lithodiversity and its spatial association with metallic mineral sites, Great Basin of Nevada. Nat. Resour. Res. 10, 209–226.
Mitchell, A.H.G., 1973. Metallogenic belts and angle of dip of Benioff zones. Nature 245, 49–52.
Mohajjel, M., Fergusson, C.L., 2000. Dextral transpression in Late Cretaceous continental collision, Sanandaj–Sirjan zone, western Iran. J. Struct. Geol. 22, 1125–1139.
Moon, C.J., 1999. Towards a quantitative model of downstream dilution of point source geochemical anomalies. J. Geochem. Explor. 65, 111–132.
Nykänen, V., Lahti, I., Niiranen, T., Korhonen, K., 2014. Receiver operating characteristics (ROC) as validation tool for prospectivity models — a magmatic Ni–Cu case study from the Central Lapland Greenstone Belt, Northern Finland. Ore Geol. Rev. http://dx.doi.org/10.1016/j.oregeorev.2014.09.007.
Parsa, M., Maghsoudi, A., Yousefi, M., Sadeghi, M., 2016. Prospectivity modeling of porphyry–Cu deposits by identification and integration of efficient mono-elemental geochemical signatures. J. Afr. Earth Sci. 114, 228–241.
Pirajno, F., 2010. Intracontinental strike-slip faults, associated magmatism, mineral systems and mantle dynamics: examples from NW China and Altay-Sayan (Siberia). J. Geodyn. 50, 325–346.
Pison, G., Rousseeuw, P.J., Filzmoser, P., Croux, C., 2003. Robust factor analysis. J. Multivar. Anal. 84, 145–172.
Porwal, A., Carranza, E.J.M., Hale, M., 2003. Knowledge-driven and data-driven fuzzy models for predictive mineral potential mapping. Nat. Resour. Res. 12, 1–25.
Porwal, A., Carranza, E.J.M., Hale, M., 2004. A hybrid neuro-fuzzy model for mineral potential mapping. Math. Geol. 36, 803–826.
Porwal, A., Carranza, E.J.M., Hale, M., 2006. A hybrid fuzzy weights-of-evidence model for mineral potential mapping. Nat. Resour. Res. 15, 1–15.
Qu, X.M., Hou, Z.Q., Zaw, K., Li, Y.G., 2007. Characteristics and genesis of Gangdese porphyry copper deposits in the southern Tibetan Plateau: preliminary geochemical and geochronological results. Ore Geol. Rev. 31, 205–223.
Reimann, C., Filzmoser, P., 2000. Normal and lognormal data distribution in geochemistry: death of a myth. Consequences for the statistical treatment of geochemical and environmental data. Environ. Geol. 39, 1001–1014.
Reimann, C., Filzmoser, P., Garrett, R.G., 2002. Factor analysis applied to regional geochemical data: problems and possibilities. Appl. Geochem. 17, 185–206.
Richards, J.P., Spell, T., Rameh, E., Razique, A., Fletcher, T., 2012. High Sr/Y magmas reflect arc maturity, high magmatic water content, and porphyry Cu ± Mo ± Au potential: examples from the Tethyan Arcs of Central and Eastern Iran and Western Pakistan. Econ. Geol. 107, 295–332.
Sadeghi, M., Morris, G.A., Carranza, E.J.M., Ladenberger, A., Andersson, M., 2013. Rare earth element distribution and mineralization in Sweden: an application of principal component analysis to FOREGS soil geochemistry. J. Geochem. Explor. 133, 160–175.
Sadeghi, M., Billay, A., Carranza, E.J.M., 2015. Analysis and mapping of soil geochemical anomalies: implications for bedrock mapping and gold exploration in Giyani area, South Africa. J. Geochem. Explor. 154, 184–193.
Sillitoe, R.H., 1972. A plate tectonic model for the origin of porphyry copper deposits. Econ. Geol. 67, 184–197.
Sillitoe, R.H., 2010. Porphyry copper systems. Econ. Geol. 105, 3–41.
Singer, D.A., Berger, V.I., Moring, B.C., 2005. Porphyry copper deposits of the world: database, map, grade and tonnage models. U.S. Geol. Surv. Open File Rep. 1005–1060.
Sotnikov, V.I., Sorokin, A.A., Ponomarchuk, V.A., Gimon, V.O., Sorokin, A.P., 2007. Porphyry Cu–Mo–(Au) mineralization: the age and relationship with igneous rock complexes of the Borgulikan ore field (upper-Amur region). Russ. Geol. Geophys. 48, 177–184.
Spadoni, M., 2006. Geochemical mapping using a geomorphologic approach based on catchments. J. Geochem. Explor. 90, 183–196.
Spadoni, M., Cavarretta, G., Patera, A., 2004. Cartographic techniques for mapping the geochemical data of stream sediments: the "sample catchment basin" approach. Environ. Geol. 45, 593–599.
Sun, X., Deng, J., Gong, Q., Wang, Q., Yang, L., Zhao, Z., 2009. Kohonen neural network and factor analysis based approach to geochemical data pattern recognition. J. Geochem. Explor. 103, 6–16.
Swets, J.A., 1988. Measuring the accuracy of diagnostic systems. Science 240, 1285–1293.
Thompson, M., Howarth, R.J., 1976. Duplicate analysis in geochemical practice. Part 1: theoretical approach and estimation of analytical reproducibility. Analyst 101, 690–698.
Treiblmaier, H., Filzmoser, P., 2010. Exploratory factor analysis revisited: how robust methods support the detection of hidden multivariate data structures in IS research. Inf. Manag. 47, 197–207.
Van Loon, A.J., 2002. The complexity of simple geology. Earth Sci. Rev. 59, 287–295.
Wang, H., Zuo, R., 2015. A comparative study of trend surface analysis and spectrum—area multifractal model to identify geochemical anomalies. J. Geochem. Explor. 155, 84–90.
Wang, W., Zhao, J., Cheng, Q., Liu, J., 2012. Tectonic–geochemical exploration modeling for characterizing geo-anomalies in southeastern Yunnan district, China. J. Geochem. Explor. 122, 71–80.
Wang, C., Carranza, E.J.M., Liu, X., Zhang, S., Da, Z., Yang, L., Sun, X., Duan, C., 2013. Characterization of primary geochemical haloes for gold exploration at the Huanxiangwa gold deposit, China. J. Geochem. Explor. 124, 40–58.
Wang, W., Zhao, J., Cheng, Q., 2014. Mapping of Fe mineralization-associated geochemical signatures using logratio transformed stream sediment geochemical data in eastern Tianshan, China. J. Geochem. Explor. 141, 6–14.
Weixuan, F., Shefeng, Y., Zhengtao, L., Baochen, Z., 2007. Geochemical characteristics and significance of major elements, trace elements and REE in mineralized altered rocks of large-scale Tsagaan Suvarga Cu–Mo porphyry deposit in Mongolia. J. Rare Earths 25, 759–769.
Xie, S., Cheng, Q., Xing, X., Bao, Z., Chen, Z., 2010. Geochemical multifractal distribution patterns in sediments from ordered streams. Geoderma 160, 36–46.
Yang, Z., Hou, Z., White, N.C., Chang, Z., Li, Z., Song, Y., 2009. Geology of the postcollisional porphyry copper–molybdenum deposit at Qulong, Tibet. Ore Geol. Rev. 36, 133–159.
Yilmaz, H., 2003. Geochemical exploration for gold in western Turkey: success and failure. J. Geochem. Explor. 80, 117–135.
Yousefi, M., Carranza, E.J.M., 2015a. Fuzzification of continuous-value spatial evidence for mineral prospectivity mapping. Comput. Geosci. 74, 97–109.
Yousefi, M., Carranza, E.J.M., 2015b. Prediction-area (P-A) plot and C-A fractal analysis to classify and evaluate evidential maps for mineral prospectivity modeling. Comput. Geosci. 79, 69–81.
Yousefi, M., Carranza, E.J.M., 2015c. Geometric average of spatial evidence data layers: A GIS-based multi-criteria decision-making approach to mineral prospectivity mapping. Comput. Geosci. 83, 72–79.
Yousefi, M., Carranza, E.J.M., 2016. Data-driven index overlay and Boolean logic mineral prospectivity modeling in Greenfield exploration. Nat. Resour. Res. 25, 3–18.
Yousefi, M., Nykänen, V., 2016. Data-driven logistic-based weighting of geochemical and geological evidence layers in mineral prospectivity mapping. J. Geochem. Explor. 164, 94–106.
Yousefi, M., Kamkar-Rouhani, A., Carranza, E.J.M., 2012. Geochemical mineralization probability index (GMPI): a new approach to generate enhanced stream sediment geochemical evidential map for increasing probability of success in mineral potential mapping. J. Geochem. Explor. 115, 24–35.
Yousefi, M., Carranza, E.J.M., Kamkar-Rouhani, A., 2013. Weighted drainage catchment basin mapping of stream sediment geochemical anomalies for mineral potential mapping. J. Geochem. Explor. 128, 88–96.
Yousefi, M., Kamkar-Rouhani, A., Carranza, E.J.M., 2014. Application of staged factor analysis and logistic function to create a fuzzy stream sediment geochemical evidence layer for mineral prospectivity mapping. Geochem.: Explor., Environ., Anal. 14, 45–58.
Zarasvandi, A., Rezaei, M., Sadeghi, M., Lentz, D., Adelpour, M., Pourkaseb, H., 2015. Rare earth element signatures of economic and sub-economic porphyry copper systems in Urumieh-Dokhtar Magmatic Arc (UDMA), Iran. Ore Geol. Rev. 70, 407–423.
Zheng, Y., Sun, X., Gao, S., Wang, C., Zhao, Z., Wu, S., Wu, X., 2014. Analysis of stream sediment data for exploring the Zhunuo porphyry Cu deposit, southern Tibet. J. Geochem. Explor. 143, 19–30.
Ziaii, M., Carranza, E.J.M., Ziaii, M., 2011. Application of geochemical zonality coefficients in mineral prospectivity mapping. Comput. Geosci. 37, 1935–1945.
Zuo, R., 2011a. Decomposing of mixed pattern of arsenic using fractal model in Gangdese belt, Tibet, China. Appl. Geochem. 26, 271–273.
Zuo, R., 2011b. Identifying geochemical anomalies associated with Cu and Pb–Zn skarn mineralization using principal component analysis and spectrum—area fractal modeling in the Gangdese Belt, Tibet (China). J. Geochem. Explor. 111, 13–22.
Zuo, R., 2012. Exploring the effects of cell size in geochemical mapping. J. Geochem. Explor. 112, 357–367.
Zuo, R., Cheng, Q., Agterberg, F.P., Xia, Q., 2009. Application of singularity mapping technique to identify local anomalies using stream sediment geochemical data, a case study from Gangdese, Tibet, western China. J. Geochem. Explor. 101, 225–235.
Zuo, R., Xia, Q., Wang, H., 2013. Compositional data analysis in the study of integrated geochemical anomalies associated with mineralization. Appl. Geochem. 28, 202–211.